

MedTVT-R1: A Multimodal LLM Empowering Medical Reasoning and Diagnosis

Yuting Zhang, Kaishen Yuan, Hao Lu, Yutao Yue, Jintai Chen, Kaishun Wu[†]

The Hong Kong University of Science & Technology (Guangzhou)

yzhang430@connect.hkust-gz.edu.cn, wuks@hkust-gz.edu.cn

[†] Corresponding author

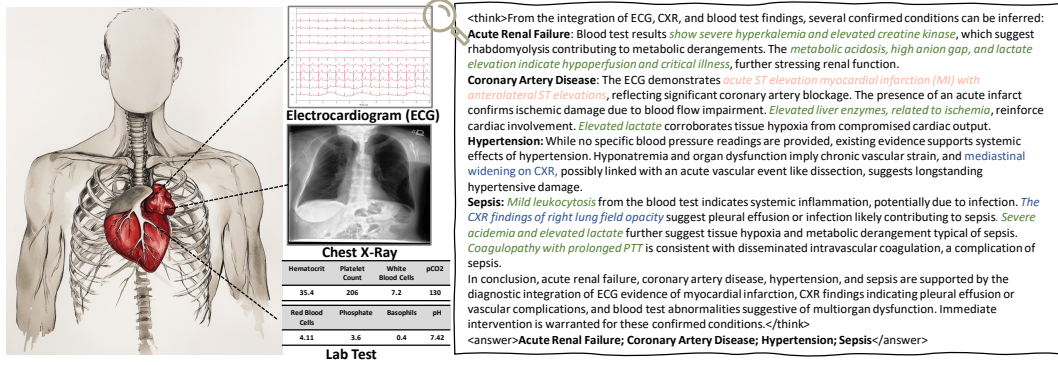


Figure 1: Overview of **MedTVT-R1**: MedTVT-R1 seamlessly integrates Electrocardiogram (Time Series), Chest X-ray (Visual Image), and Blood Test (Tabular Data) to deliver comprehensive long-text **Medical** reasoning and diagnosis across various diseases.

Abstract

Accurate and interpretable multi-disease diagnosis remains a critical challenge in medical research, particularly when leveraging heterogeneous multimodal medical data. Current approaches often rely on single-modal data, limiting their ability to comprehensively understand complex diseases. To address this, we propose MedTVT-R1, a novel Multimodal Large Language Model (MLLM) framework designed to integrate clinical multimodal data for reasoning and diagnosing multiple diseases. We construct MedTVT-QA, a curated instruction dataset that provides question-answer pairs for physiological-level interpretations and disease-level diagnoses with a Chain of Evidence approach. MedTVT-R1 incorporates a modality perception layer to capture inter-modal dependencies and adaptively weight modality contributions. Additionally, we employ Group Relative Policy Optimization (GRPO)-based Reinforcement Fine-Tuning with a Jaccard Reward function to enhance diagnostic reasoning. Experimental results demonstrate MedTVT-R1’s superiority in multimodal feature utilization and multi-disease diagnosis, offering significant potential for clinical applications such as diagnostic report generation and comorbidity reasoning. The dataset and code are available at <https://github.com/keke-nice/MedTVT-R1>.

1 Introduction

The rapid development of artificial intelligence (AI) has profoundly reshaped the landscape of medical research and clinical practice, especially in demonstrating significant progress and potential in medical data analysis [7, 43, 20, 55] and disease diagnosis [8, 15], with an extensive impact [13].

At present, most existing studies primarily rely on single-modal medical data to perform disease diagnosis [9, 20, 63, 4]. Although these single-modal approaches demonstrate certain effectiveness within their respective specific domains, their perception of physiology is often too limited to offer a holistic and comprehensive understanding of complex diseases. Taking diabetes as an example, its physiological manifestations are typically reflected across multiple modalities, such as altered heart rate variability in electrocardiograms (ECG), pulmonary complications observable in chest X-rays (CXR), and abnormal glucose or lipid levels revealed by laboratory blood tests (LAB) [38]. Therefore, to address the risk of incomplete or inaccurate diagnoses resulting from reliance on a single modality, it is essential to integrate multimodal medical data for comprehensive and in-depth analysis of complex diseases [3, 53].

Consequently, there are a number of efforts that have emerged to explore leveraging multimodal medical data for disease diagnosis [27, 53, 60, 1]. Nevertheless, these methods often make only simple and direct determinations about the presence or absence of a specific disease [18, 28], but struggle with performing robust long-text diagnostic reasoning and generating interpretable clinical insights for multiple diseases, which severely hinders their practical application.

Recently, multimodal large language models (MLLMs) [67, 35, 41, 42, 59, 61] have undergone rapid development and achieved impressive results in a variety of tasks, such as vision-language and audio-language tasks. They have demonstrated strong capabilities in integrating, generalizing, and reasoning across diverse data modalities, offering promising potential for generating interpretable disease diagnosis reports from medical data. Although several pioneering studies have made preliminary attempts to apply MLLMs in the medical field, such as for ECG analysis [69, 58] or medical image reporting [52, 39, 57] tasks, these works are still limited to single modalities (*e.g.*, ECG, CXR) and remain at physiological-level understanding rather than disease-level reasoning. Therefore, an MLLM that can perceive and integrate heterogeneous multimodal medical data, thereby enabling interpretable multi-disease reasoning and diagnosis, remains a significant gap in current research.

Based on the observations above, we propose a novel MLLM framework, named **MedTVT-R1**, which leverages the complementarity and mutual corroboration of clinical multimodal medical data to enable reasoning and diagnosis of multiple complex diseases, with its advancements illustrated in Figure 1. To achieve this, we innovatively construct a well-curated instruction dataset, **MedTVT-QA**, which is the first attempt to simultaneously consider three heterogeneous modalities (*i.e.*, ECG, CXR, and LAB), and provides corresponding question-answer (QA) pairs that not only cover physiological-level interpretations, but further explore disease-level diagnoses based on a Chain of Evidence (CoE) that fully leverages the complementarity and mutual corroboration among modalities, thereby establishing a solid foundation for MLLMs to progressively integrate multimodal medical data for physiological perception and multi-disease diagnosis. Moreover, we introduce a modality perception layer (MPL) for MedTVT-R1, which can effectively capture the dependencies among different modalities and adaptively weight their contributions based on the relevance of each modality to specific diseases, thereby maximizing cross-modal interaction and information utilization.

To further unlock the potential of the constructed data, inspired by DeepSeek-R1 [19], we also adopt Reinforcement Fine-Tuning (RFT) based on Group Relative Policy Optimization (GRPO) for post-training, with a dedicated Jaccard Reward function for multi-disease diagnostic scenarios, which substantially enhances the model’s reasoning capability. Extensive experiments demonstrate the superiority of the proposed MedTVT-R1 in physiological-level understanding for each modality as well as in effectively leveraging multimodal features for disease-level diagnosis, which holds significant implications for applying MLLMs in clinical scenarios such as interpretable diagnostic report generation and complex comorbidity reasoning. Our contributions are summarized as follows:

- We introduce MedTVT-QA, the first medical instruction dataset that features heterogeneous modalities including ECG (Time Series), CXR (Visual Images), and LAB (Tabular Data), and offers QA pairs covering both physiological-level understanding and disease-level diagnosis with a Chain of Evidence, thus establishing a solid foundation for MLLMs to seamlessly integrate multimodal medical data for disease reasoning and diagnosis.

- We propose MedTVT-R1, a novel MLLM framework that fully leverages the complementarity and mutual corroboration among clinical multimodal data for interpretable diagnosis of complex comorbidities, with a modality perception layer that effectively captures inter-modal dependencies and adaptively weights the contribution of each modality.
- We employ a Reinforcement Fine-Tuning (RFT) strategy based on Group Relative Policy Optimization (GRPO) incorporating a dedicated Jaccard reward function to unlock data potential and enhance the model’s reasoning accuracy.
- Extensive experiments demonstrate that MedTVT-R1 achieves state-of-the-art performance in physiological representation understanding across various modalities and multimodal diagnosis and report generation for comorbidity.

2 Related Work

MLLM for Medical Diagnosis. The application of Multimodal Large Language Models (MLLMs) in medical diagnosis has gained significant attention due to their ability to process and integrate diverse data modalities, such as text [36, 37, 24, 14, 66], images [23, 32, 31, 46], and tabular data [6, 22]. Early works focused on single-modal approaches, such as text-based models for clinical note analysis [24, 66, 37], image-based models for radiology interpretation [32, 23], or ECG-based models for cardiac status analysis [69, 65, 30, 62]. Although significant advancements have been made, existing research has yet to integrate Time series data (e.g., Electrocardiograms), Visual data (e.g., chest X-rays), and Tabular data (e.g., lab results) into a unified framework for comprehensive Medical disease analysis and diagnosis. To bridge this gap, we introduce **MedTVT-R1**, a multimodal large language model designed to seamlessly combine CXR, ECG, and lab data through cross-modal interactions and contribution-aware operator, enabling accurate and interpretable disease diagnosis.

Reinforcement Learning with Verifiable Rewards. Group Relative Policy Optimization (GRPO) [19], unlike Proximal Policy Optimization (PPO) [64, 50] which estimates advantages through a reward model, approximates advantages by obtaining multiple samples from the LLM using the same prompt, with the advantage being the normalized reward for each response within its set of generated responses, achieving notable success in text-based tasks [51, 48, 10] such as summarization and dialogue generation, as well as vision tasks [44, 56] like image captioning. Recently, GRPO has been applied to medical image analysis [29, 47]. However, it has not yet been utilized for multimodal tasks in the crucial area of multi-disease diagnosis, which requires the integration of text, images, time series, and tabular data. In this work, we are pioneering the application of GRPO with a newly designed reward function, the Jaccard Reward, to enhance the accuracy of multi-disease prediction.

3 Methodology

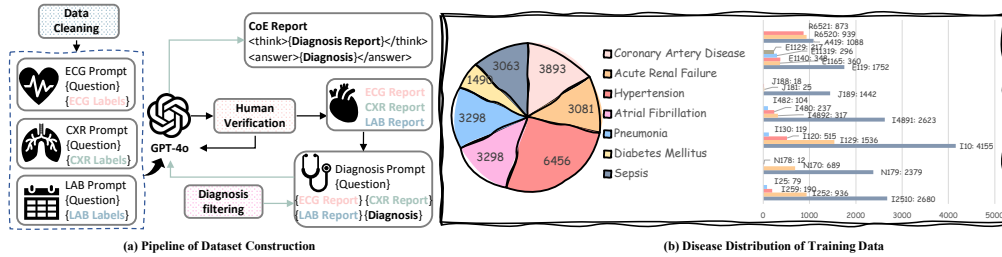


Figure 2: MedTVT-QA dataset construction and disease distribution. (a) Pipeline of Dataset Construction: labels are refined to ensure consistency, prompts guide GPT-4o in generating verified physiological-level reports, which are combined with diagnostic labels to produce disease-level reports. Diagnostic labels are organized into seven primary categories with detailed subtypes. (b) Disease distribution of MedTVT-QA, with subtypes classified by ICD-10 codes. More details can be found in Appendix B.

3.1 MedTVT-QA

To equip MLLMs with the ability to perform physiological understanding and disease diagnosis leveraging heterogeneous multimodal medical data, we collect raw medical data conforming to clinical temporal logic from the MIMIC-IV dataset, thanks to Symile [49]. Specifically, for each patient, we acquire electrocardiogram (ECG) readings and blood test results within the first 24 hours

of hospital admission (from MIMIC-IV-ECG [16] and MIMIC-IV [25]), as well as chest X-ray (CXR) images taken within 24 to 72 hours post-admission (from MIMIC-CXR-JPG [26]), ultimately forming a total of 8,706 multimodal data combinations with consistent physiological temporal sequences, of which 8,331 for training and 375 for testing. Besides, the MIMIC-IV-ECG-EXT-ICD [54] dataset provides emergency department and hospital discharge diagnoses, which are linked to the MIMIC-IV dataset. Based on these raw data, we progressively construct multimodal question-answer (QA) pairs from the perspectives of physiological-level representation analysis and disease-level diagnostic reasoning, with the entire process shown in Figure 2 (a), which will be introduced in detail below.

QA Pairs on Physiological-level Representation Analysis.

To enable MLLMs to acquire a basic comprehension of the physiological meanings represented by each modality, *i.e.*, ECG, CXR, and LAB, and to lay the groundwork for subsequent multi-disease reasoning and diagnosis based on multimodal data, we first construct QA pairs focused on physiological-level analysis for each modality. Specifically, taking the ECG modality as an example, we design a rigorous prompt with reference to physiological-level annotations, which consists of Role Setting, Task Description, Answer Guidance, and Answer Format to instruct GPT-4o [2], as outlined below:

Role Setting: You are a renowned cardiologist with expertise in interpreting electrocardiograms (ECGs).
Task Description: The ECG analysis has yielded the following labels: {labels}. Based on these labels, please address the question: {question}.
Answer Guidance: Your response should incorporate all relevant labels, excluding any unrelated ones. Provide a synthesis of the labels, focusing on clinical significance.
Answer Format: Begin with a brief introduction to your analysis. Provide detailed explanations for each specific ECG label. Offer a concise summary.

Here, {labels} refers to physiological-level annotations for the ECG data, such as Sinus Rhythm or Left Bundle Branch Block. {question} is randomly sampled from several carefully crafted question templates, such as ‘What information can be derived from the ECG?’. An example of a constructed QA pair that summarizes and analyzes the physiological representations encompassed in ECG is:

Question: What information can be derived from the ECG <ecg>?
Answer: ECG Analysis: Upon evaluating the electrocardiogram (ECG), the following observations can be made:
 1. Sinus Rhythm: The heart is under the control of the sinoatrial (SA) node, which is the natural pacemaker. This finding suggests that the electrical activity of the heart is originating from the SA node and progressing through the normal conduction pathway, leading to a regular rhythm. This is a foundational indicator of organized cardiac activity.
 2. Left Bundle Branch Block (LBBB): There is evidence of delayed or disrupted conduction through the left bundle of the heart’s electrical conduction system. This results in a characteristic pattern on the ECG, with a widened QRS complex (>120 ms) and specific morphologies in leads, such as a broad, notched appearance in V5-V6 and an absence of normal septal depolarization. LBBB may occur in conditions like ischemic heart disease, cardiomyopathy, or hypertension-induced structural changes, though it can also occasionally be found in asymptomatic individuals.
 Summary: The heart demonstrates a sinus rhythm, indicating normal initiation of electrical activity. However, the presence of a left bundle branch block signifies an abnormality in electrical conduction, often associated with underlying cardiac pathology. As a whole, this ECG is classified as abnormal due to the conduction disturbance, warranting further investigation to assess structural or functional cardiac issues.

Similar prompts are also applied to CXR and LAB data to organize the corresponding physiological-level QA pairs for each modality. It is worth noting that, for LAB data, we group 50 common laboratory indicators into seven categories according to their physiological significance to facilitate processing. The content generated above for physiological-level representation analysis undergoes manual review and revision by professionals to ensure its rationality and reliability. More details on physiological-level annotation and examples of QA pairs for each modality can be found in the Appendix A to C.

QA Pairs on Disease-level Diagnostic Reasoning. Building upon the aforementioned completed physiological-level representation analysis for each modality, we further construct QA pairs that fully integrate information across modalities and conduct disease-level diagnostic reasoning, thereby enhancing the capability of MLLMs to handle complex multiple diseases. We focus on seven common and clinically significant diseases for which supporting evidence can be found in ECG, CXR, and LAB data, including *Coronary Artery Disease*, *Acute Renal Failure*, *Hypertension*, *Atrial Fibrillation*, *Pneumonia*, *Diabetes Mellitus*, and *Sepsis*, each of which contains several subtypes, with details in the Appendix B. The corresponding statistics are presented in Figure 2 (b). We also employ a four-element prompt with reference to disease-level annotations to instruct GPT-4o, and compel its response to include a Chain of Evidence (CoE) to fully leverage the complementarity and mutual corroboration among modalities, thereby thoroughly extracting multimodal evidence for disease diagnosis, as follows:

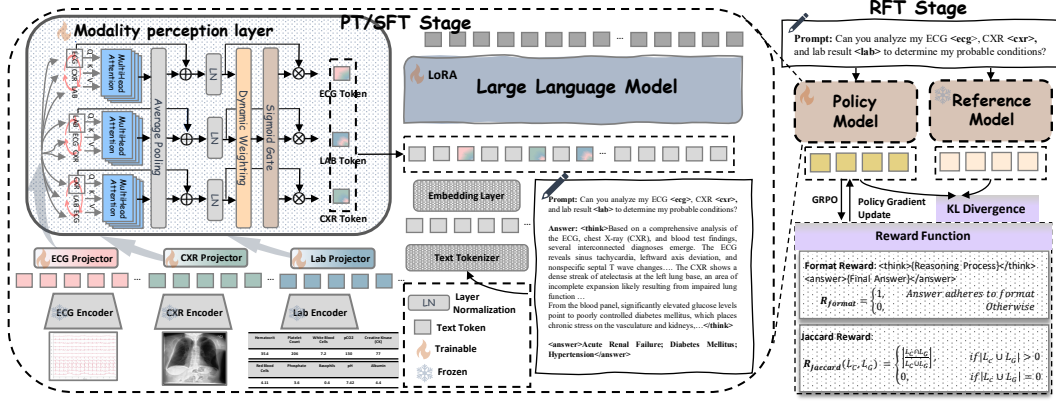


Figure 3: Pipeline of MedTVT-R1. Pretraining processes ECG, CXR, and LAB data through encoders and projectors, combined with prompts, to train projectors and LLM’s LoRA for enhanced physiological understanding. The SFT stage adds a Modality Perception Layer for interaction and integration, refining disease analysis. The RFT stage applies GRPO, using the SFT-trained model for policy and inference, optimizing KL divergence and reward loss.

Role Setting: You are a renowned diagnostician with expertise in integrating ECG, CXR, and blood test results.

Task Description: The following diagnostics have been provided:

- ECG Analysis: {ecg_report}
- CXR Analysis: {cxr_report}
- Blood Test Analysis: {blood_test_report}
- Diseases: {result_diseases}

You need to pretend that the ECG, CXR, and blood test analyses are based on your interpretation of the raw data, and the final diagnosis is your synthesis of these three diagnostic methods, please address the question: {question}

Answer Guidance: Please find definitive evidence from the ECG, CXR, and blood test results, leveraging the complementarity and mutual corroboration of these three modalities, to robustly prove the reasons why the patient has the diseases I provided. Your response must include every disease I provided, using the exact wording I provided, and you must not mention any diseases other than those I provided. Please make sure to provide evidence for these diagnoses! These are confirmed conditions.

Answer Format: <think>[Diagnostic evidence synthesized from the three modalities]</think>\n <answer>{disease1; disease2; ...}</answer>

Here, {ecg_report}, {cxr_report}, and {blood_test_report} respectively represent the physiological-level analyses of the three modalities. {result_diseases} refers to the disease-level annotation of the sample. {question} is randomly sampled from several carefully crafted question templates, such as ‘Can you analyze my ECG, CXR and lab result to determine my probable conditions?’. The CoE is implemented by ‘Please find definitive evidence...’. The content obtained in this process is also reviewed by professionals to enhance its trustworthiness. An example of a QA pair that integrates multimodal information to mine evidence for multi-disease reasoning and diagnosis is shown in Figure 3, and the complete version is provided in the Appendix D.

3.2 MedTVT-R1

Based on the meticulously constructed MedTVT-QA dataset described above, we propose MedTVT-R1, an MLLM framework capable of fully exploiting the complementarity and mutual corroboration of multimodal medical data for interpretable multi-disease reasoning and clinical diagnosis. In the following, we will introduce the model architecture and training strategy of MedTVT-R1 in detail.

3.2.1 Architecture

The proposed MedTVT-R1 mainly consists of modality-specific encoders and projectors, a Modality Perception Layer (MPL), and a Large Language Model (LLM), with its overall architecture illustrated on the left side of Figure 3. Given the raw data of ECG signals $\mathbf{X}_E \in \mathbb{R}^{N \times L}$, CXR images $\mathbf{X}_C \in \mathbb{R}^{C \times H \times W}$, and LAB tables $\mathbf{X}_L \in \mathbb{R}^{N'}$, they are first processed by their respective modality-specific encoders for feature extraction, and then the encoded features are fed into modality-specific projectors to a shared dimension d for alignment and compatibility with the textual embedding space of the LLM, facilitating seamless integration between multimodal features and textual tokens; this process can be formulated as follows:

$$\mathbf{Z}_E = g_E(f_E(\mathbf{X}_E)) \in \mathbb{R}^d, \quad \mathbf{Z}_C = g_C(f_C(\mathbf{X}_C)) \in \mathbb{R}^d, \quad \mathbf{Z}_L = g_L(f_L(\mathbf{X}_L)) \in \mathbb{R}^d, \quad (1)$$

where $\mathbf{Z}_{E/C/L}$ denotes the projected multimodal features, and $f_{E/C/L}$ and $g_{E/C/L}$ represent the modality-specific encoders and projectors, respectively.

Subsequently, to enable efficient interaction and fusion among modalities, we introduce a Modality Perception Layer (MPL), which comprises a Cyclic Multi-Head Attention (CMHA) mechanism and a Contribution-Aware Operator (CAO). Specifically, the projected features \mathbf{Z}_E , \mathbf{Z}_C , and \mathbf{Z}_L are first processed by the CMHA mechanism, in which each modality feature cyclically serves as the Query, Key, and Value to compute multi-head attention, enabling comprehensive capture of cross-modal dependencies and facilitating in-depth information exchange among ECG, CXR, and LAB features. After one round of cycling, the outputs are fused through average pooling, while a residual connection is employed to preserve modality-specific information. This process can be formulated as follows:

$$\mathbf{F} = \text{AveragePooling}(\text{CMHA}(\mathbf{Z}_E, \mathbf{Z}_C, \mathbf{Z}_L)), \quad \mathbf{M}_{E/C/L} = \mathbf{Z}_{E/C/L} + \mathbf{F}, \quad (2)$$

where $\mathbf{M}_{E/C/L}$ denotes the updated features of each modality, which encapsulate both modality-specific and modality-shared information. Recognizing that each modality contributes in varying degrees to the reasoning and diagnosis of various diseases, for example, ECG features are relatively more important for detecting Coronary Artery Disease, we design a Contribution-Aware Operator that adaptively assigns weights to the features of each modality based on the diagnostic context, which can be formulated as follows:

$$\mathbf{T}_E, \mathbf{T}_C, \mathbf{T}_L = \sigma(h[\mathbf{M}_E : \mathbf{M}_C : \mathbf{M}_L]) \otimes (\mathbf{M}_E, \mathbf{M}_C, \mathbf{M}_L), \quad (3)$$

where $[\cdot]$ denotes the concatenation operation, h is a learnable transformation matrix, σ represents the Sigmoid activation, and \otimes denotes element-wise multiplication. The final multimodal features \mathbf{T}_E , \mathbf{T}_C , and \mathbf{T}_L are used to replace the placeholders $\langle \text{ecg} \rangle$, $\langle \text{cxr} \rangle$, and $\langle \text{lab} \rangle$ in the text tokens, which are obtained by processing the input prompt through the tokenizer and embedding layer. An example input prompt could be: ‘What illnesses might be indicated by the findings from my ECG $\langle \text{ecg} \rangle$, CXR $\langle \text{cxr} \rangle$, and blood work $\langle \text{lab} \rangle$?’. The resulting sequence $\mathbf{T}_{\text{input}} = \{\mathbf{T}_Q, \mathbf{T}_E, \mathbf{T}_C, \mathbf{T}_L, \mathbf{T}_A\}$ is then fed into the LLM, where \mathbf{T}_Q and \mathbf{T}_A are derived from the QA pairs in the MedTVT-QA dataset.

3.2.2 Training Strategy

We employ a three-stage training strategy for MedTVT-R1, which includes Pre-training (PT), Supervised Fine-Tuning (SFT), and Reinforcement Fine-Tuning (RFT), to progressively enhance its ability to perceive the physiological representations of each modality and integrate multimodal information for interpretable multi-disease reasoning and diagnosis.

Pre-training. With the aim of helping the model form an initial understanding and awareness of the physiological significance across all modalities, we first perform pre-training using physiological-level QA pairs from the MedTVT-QA dataset. During this stage, the projectors and the Low-Rank Adaptation (LoRA) modules embedded in the LLM are set as trainable, while the other components remain frozen. Notably, the MPL module is absent at this stage as no cross-modal interaction is involved. The optimization objective is to maximize the likelihood of generating the target response tokens, formalized as:

$$\mathcal{L}_{\text{PT}} = -\mathbb{E}_{(\mathbf{T}_Q, \mathbf{T}_{E/C/L}, \mathbf{T}_A) \sim \mathcal{D}} \sum_{t=1}^T \log \pi_{\theta}(y_t \mid \mathbf{T}_Q, \mathbf{T}_{E/C/L}, y_{<t}), \quad (4)$$

where $\pi_{\theta}(y_t \mid \cdot)$ denotes the conditional probability of generating the t -th token y_t , given the prompt, modality features, and the previously generated tokens $y_{<t}$.

Supervised Fine-Tuning. With the pretrained model that already demonstrates a solid understanding of the physiological significance of each modality, we further conduct SFT based on disease-level QA pairs with CoE logic from the MedTVT-QA dataset to equip the model with the capability to synthesize multimodal representations and uncover the complementarity and mutual corroboration among modalities for multi-disease reasoning and diagnosis. During this stage, the MPL and the LoRA modules embedded in the LLM are set to be trainable while the other components remain frozen, and the optimization objective is similar to that of the pre-training stage, namely:

$$\mathcal{L}_{\text{SFT}} = -\mathbb{E}_{(\mathbf{T}_Q, \mathbf{T}_E, \mathbf{T}_C, \mathbf{T}_L, \mathbf{T}_A) \sim \mathcal{D}} \sum_{t=1}^T \log \pi_{\theta}(y_t \mid \mathbf{T}_Q, \mathbf{T}_E, \mathbf{T}_C, \mathbf{T}_L, y_{<t}). \quad (5)$$

Reinforcement Fine-Tuning. To unlock the potential of the constructed dataset and boost the model’s reasoning performance, inspired by the advancements of DeepSeek-R1, we perform RFT using Group

Method	LLM	NLG				CE			
		BLEU	METEOR	ROUGE	BERT	PRECISION	RECALL	F1 SCORE	AUC
InternVL3-1B [70]	InternVL3-1B	0.0178	0.1884	0.1265	0.8188	0.3333	0.1333	0.1904	0.5053
LLaVA-1.5-7B [40]	Vicuna-7B	0.0029	0.0809	0.0681	0.7796	0.2495	0.1279	0.1691	0.5004
LLaVA-One-Vision-7B [34]	Qwen2-7B	0.0144	0.1618	0.1168	0.8016	0.3120	0.1247	0.1782	0.4975
Qwen2.5-VL-3B-Instruct [5]	Qwen2.5-3B-Instruct	0.0218	0.2031	0.1331	0.8181	0.3493	0.1397	0.1995	0.5000
Mini-InternVL-Chat-2B-V1-5 [5]	InternLM2-Chat-1.8B	0.0092	0.1347	0.0959	0.8008	0.2176	0.1343	0.1661	0.5015
Molmo-7B-O-0924 [11]	OLMo-7B	0.0155	0.1456	0.1070	0.8028	0.0295	0.0608	0.0398	0.5001
Deepseek-VL-1.3B-Chat [45]	Deepseek-1.3B-Chat	0.0341	0.1756	0.1435	0.8128	0.2510	0.1278	0.1534	0.5021
LLaVA-NeXT-8B [33]	LLaMA3-8B	0.0145	0.1532	0.1067	0.8145	0.2674	0.1294	0.1567	0.4987
MedTVT-R1 w/o PT	LLaMA3.2-1B	0.1131	0.3280	0.2043	0.8599	0.4980	0.5208	0.4672	0.5851
MedTVT-R1 w/o RFT	LLaMA3.2-1B	0.1325	0.3499	0.2261	0.8660	0.5237	0.5783	0.4992	0.6242
MedTVT-R1	LLaMA3.2-1B	0.1353	0.3536	0.2295	0.8652	0.5407	0.5908	0.5190	0.6554

Table 1: Comparison of MedTVT-R1 with various MLLMs and its variants on disease-level reasoning and diagnostic capabilities.

Relative Policy Optimization (GRPO) under the Reinforcement Learning with Verifiable Rewards (RLVR) framework. The training corpus and trainable components remain consistent with those in the SFT stage. The optimization objective can be formulated as:

$$\max_{\pi_{\theta}} \mathbb{E}_{\mathbf{A} \sim \pi_{\theta}(\mathbf{Q})} [R_{\text{RLVR}}(\mathbf{Q}, \mathbf{A})] = [R(\mathbf{Q}, \mathbf{A}) - \beta \text{KL}[\pi_{\theta}(\mathbf{A} | \mathbf{Q}) \| \pi_{\text{ref}}(\mathbf{A} | \mathbf{Q})]], \quad (6)$$

where π_{θ} and π_{ref} are the policy model and the reference model, respectively. R is the verifiable reward function. $\text{KL}[\pi_{\theta}(\mathbf{A} | \mathbf{Q}) \| \pi_{\text{ref}}(\mathbf{A} | \mathbf{Q})]$ penalizes divergence from the reference policy π_{ref} , ensuring both correctness and alignment with prior knowledge. The hyperparameter β controls the trade-off between reward maximization and policy regularization.

GRPO directly compares the relative quality of responses within a group without requiring an additional critic model. Specifically, given a question \mathbf{Q} , GRPO first generates G candidate responses $\{o_1, o_2, \dots, o_G\}$ according to the current policy $\pi_{\theta_{\text{old}}}$, which are then assigned rewards $\{r_1, r_2, \dots, r_G\}$. The relative quality of these responses is calculated by normalizing the rewards using their mean and standard deviation. GRPO encourages the model to prioritize responses with higher relative rewards, fostering improved performance without requiring a separate critic.

The verifiable reward function R consists of the Format Reward and the Jaccard Reward, *i.e.*, $R = R_F + R_J$, ensuring both prediction accuracy and structural consistency. In line with DeepSeek-R1, the Format Reward R_F is used to enforce the model’s compliance with predefined formatting rules for the `<think>` and `<answer>` tags. The Jaccard Reward R_J is a novel, meticulously designed reward function tailored for multi-disease diagnosis, which evaluates the alignment between the model’s predictions and the ground truth by leveraging the Jaccard similarity coefficient, thereby quantifying the overlap between the predicted and actual disease sets. Specifically, for each model completion and its corresponding ground truth, the disease sets within the `<answer>` tags are first extracted using regular expressions and denoted as $L_C = \{l_{c_1}, l_{c_2}, \dots, l_{c_m}\}$ and $L_G = \{l_{g_1}, l_{g_2}, \dots, l_{g_n}\}$, where l_{c_i} and l_{g_j} represent individual diseases in the predicted and ground truth sets, respectively. The Jaccard Reward R_J is then computed as:

$$R_J(L_C, L_G) = \begin{cases} \frac{|L_C \cap L_G|}{|L_C \cup L_G|}, & \text{if } |L_C \cup L_G| > 0, \\ 0, & \text{if } |L_C \cup L_G| = 0. \end{cases} \quad (7)$$

When the union of the sets is not empty, the R_J is determined by the ratio of the intersection size to the union size, thereby capturing the degree of overlap between the prediction and ground truth. If the union is empty, the R_J is set to zero to ensure robustness against invalid or incomplete outputs. Therefore, the Jaccard reward encourages the model to generate outputs that are highly consistent with the ground truth labels, which effectively helps improve both the accuracy and reliability in multi-disease diagnosis scenarios.

4 Experiments

4.1 Training Details and Metrics

Training Details.

We conduct all experiments on a server equipped with eight NVIDIA A800 80GB GPUs. For the LLM, we choose LLaMA 3.2-1B [17] and integrate the LoRA modules [21] with a rank of 8 for fine-tuning. For the modality-specific encoders, we use the pre-trained weights from ECGFM-KED [58], ViT-B/16 [12], and Symile [49] for ECG, CXR, and LAB, respectively. All modality-specific projectors

Method	ECG-QA				CXR-QA				LAB-QA			
	BLEU	METEOR	ROUGE	BERT	BLEU	METEOR	ROUGE	BERT	BLEU	METEOR	ROUGE	BERT
InternVL3-1B [70]	0.0186	0.1795	0.1379	0.8282	0.0239	0.1827	0.1273	0.8309	0.0083	0.1234	0.0750	0.7750
LLaVA-1.5-7B [40]	0.0055	0.1084	0.0866	0.8100	0.0034	0.0967	0.0812	0.8012	0.0170	0.1402	0.1133	0.7937
LLaVA-One-Vision-7B [34]	0.0313	0.2263	0.1545	0.8322	0.0260	0.1877	0.1325	0.8214	0.0088	0.1362	0.0967	0.7883
Qwen2.5-VL-3B-Instruct [5]	0.0304	0.2483	0.1687	0.8418	0.0310	0.1798	0.1261	0.8230	0.0081	0.1129	0.0764	0.7832
Mini-InternVL-Chat-2B-V1-5 [5]	0.0102	0.1336	0.0984	0.8112	0.0088	0.1082	0.0825	0.8044	0.0085	0.1286	0.1118	0.7781
Molmo-7B-O-0924 [11]	0.0233	0.1949	0.1341	0.8305	0.0211	0.1813	0.1255	0.8231	0.0091	0.1102	0.1120	0.7587
Deepseek-VL-1.3B-Chat [45]	0.0240	0.1708	0.1162	0.8205	0.0298	0.1510	0.1312	0.8215	0.0118	0.0975	0.1184	0.7675
LLaVA-NeXT-8B [33]	0.0091	0.1412	0.1064	0.8009	0.0107	0.1305	0.1307	0.8199	0.0102	0.1057	0.1091	0.7623
MedTVT-R1	0.0831	0.3044	0.2202	0.8650	0.0931	0.3073	0.2121	0.8673	0.1807	0.3827	0.3081	0.8855

Table 2: Comparison of MedTVT-R1 with various MLLMs on physiological-level understanding and analysis capabilities.


What illnesses might be indicated by the findings from my ECG <ecg>, CXR <cxr>, and blood work <lab>?	
 MedTVT-R1	<p><think>Based on the ECG, CXR, and blood test findings, the presented diseases hypertension and pneumonia is evidenced by combining findings from these diagnostic modalities.</p> <p>Hypertension: ECG findings reveal evidence of left ventricular hypertrophy (LVH) with secondary repolarization abnormalities, left axis deviation, and intraventricular conduction defects. LVH is a common sequela of chronic hypertension, which increases left ventricular workload and myocardial strain, necessitating left ventricular thickening. <i>The left axis deviation further supports hypertensive heart changes. The CXR supports this with an enlarged cardiac silhouette consistent with hypertensive heart disease or left ventricular hypertrophy. Elevated blood pressure could contribute to the LVH seen and conduction abnormalities.</i></p> <p>Pneumonia: The CXR confirms resolution of bilateral interstitial opacities, <i>consistent with</i> prior pulmonary edema, but ongoing respiratory compromise is <i>evident</i> from elevated pCO2 and low pH in the blood tests. This <i>aligns with</i> pulmonary compromise often associated with pneumonia. Atelectasis in the right lung base suggests impaired lung aeration, which may result from infection-related processes. <i>The blood test reveals elevated white blood cell count and neutrophil dominance in the blood panel, confirming an active inflammatory or infectious process, strongly supporting the presence of pneumonia.</i> These results collectively indicate that the patient's hypertension and pneumonia are interconnected, with hypertension exacerbating cardiac stress leading to cardiac remodeling and vascular congestion evident in the CXR. <i>Pneumonia presents a plausible cause for these chronic lung changes and exacerbation of the respiratory dysfunction seen in low pH, bicarbonate, and BRAD.</i></p> <p></think></p> <p><answer>Hypertension; Pneumonia</answer></p>

Figure 4: Inference example of MedTVT-R1: Blue highlights "evidence words," while green denotes critical information extracted from various modalities.

adopt the Dense block architecture from MuMu-LLaMA [42], with the embedding dimension d set to 2048. During training, the PT and SFT stages are each trained for 20 epochs, while the RFT stage is trained for 500 iterations using the open-source Trainer framework, with G in GRPO set to 8.

Metrics. The effectiveness of multi-disease reasoning and diagnosis was evaluated from two perspectives. First, the descriptive accuracy of the generated diagnostic text was assessed using natural language generation (NLG) metrics, including BLEU, METEOR, ROUGE, and BERTScore. Second, the classification accuracy of multi-label disease categories in the responses was evaluated using clinical efficacy (CE) metrics, such as PRECISION, RECALL, F1 SCORE, and AUC.

4.2 Quantitative Analysis

Disease-level Diagnostic Reasoning Results. Since there is no multimodal large model capable of comprehensively analyzing ECG signals, medical images, and tabular data, we transform ECG signals into images and convert LAB tabular data into text, enabling feasible comparison with the existing leading MLLMs. Table 1 presents the comparison results between our proposed model, MedTVT-R1, and eight state-of-the-art MLLMs, including InternVL3-1B [70], LLaVA-1.5-7B [40], LLaVA-One-Vision-7B [34], Qwen2.5-VL-3B-Instruct [5], Mini-InternVL-Chat-2B-V1-5 [5], Molmo-7B-O-0924 [11], Deepseek-VL-1.3B-Chat [45], and LLaVA-NeXT-8B [33]. These MLLMs range in size from 1B to 8B and utilize various backbones, such as InternVL, Vicuna, OLMo, as well as Deepseek-VL, which incorporates reinforcement learning during training. All inference results were obtained using the open-source framework ModelScope SWIFT [68].

The results demonstrate that MedTVT-R1 outperforms these leading models, excelling not only in natural language generation but also in clinical evaluation. This indicates the superior capability of MedTVT-R1 in both descriptive and diagnostic reasoning tasks in multi-disease scenarios. Furthermore, Table 1 also presents ablation studies to investigate the impact of physiological-level pre-training and RFT-based post-training on the model's performance. The results show that removing either component leads to a noticeable decline in performance. Specifically, the findings highlight two key insights: 1) Physiological-level pre-training enables the model to acquire physiological knowledge across modalities in advance, which facilitates the differentiation and integration of multimodal physiological information during the subsequent SFT stage for disease-level diagnostic reasoning. 2) The RFT stage based on GRPO further unleashes the potential of the constructed data and enhances the model's multi-disease diagnostic performance, enabling deeper and more effective cross-modal reasoning.

Physiological-level Understanding Results. Similar to our analysis of Disease-level Diagnostic Reasoning, we evaluate MedTVT-R1 against eight MLLMs in terms of their single-modality un-

Table 3: The ablation of the Cyclic Multi-Head Attention (CMHA) mechanism and Contribution-Aware Operator (CAO) in the Modality Perception Layer (MPL), as well as the impact of modal missingness during the pre-training phase on the final results. Metrics include METEOR, ROUGE, RECALL, and F1 SCORE. Default settings are marked in **gray**.

(a) Ablation study of MPL.

MPL		NLG		CE	
CMHA	CAO	MET.	ROU.	REC.	F1
✗	✓	0.3455	0.2013	0.5733	0.4977
✓	✗	0.3378	0.2145	0.5826	0.4867
✓	✓	0.3536	0.2295	0.5908	0.5190

(b) Ablation study of Modalities.

Modality			NLG		CE	
ECG	CXR	LAB	MET.	ROU.	REC.	F1
✗	✓	✓	0.3245	0.2058	0.5320	0.4739
✓	✗	✓	0.3267	0.2019	0.5739	0.4869
✓	✓	✗	0.3455	0.2218	0.5845	0.5023
✓	✓	✓	0.3536	0.2295	0.5908	0.5190

derstanding capabilities at the Physiological-level. The results in Table 2 clearly demonstrate that our model outperforms all competitors. Notably, the Physiological-level representation analysis we designed is a challenging long-text generation task, requiring the generation of over 300 words per instance. Despite this complexity, MedTVT-R1 delivers outstanding results, further showcasing its advanced capabilities in handling lengthy and detailed outputs. In a horizontal comparison, the understanding of LAB tabular data is superior to that of CXR images and ECG signals. This aligns with intuitive expectations, as LAB tabular data is inherently closer to a textual format, making it easier for large language models to process compared to the other two modalities. These findings highlight the exceptional performance of MedTVT-R1 in long-text generation tasks and its ability to effectively comprehend and analyze physiological data across diverse modalities. Furthermore, the results emphasize the model’s robustness in both single-modality perception and multimodal reasoning, establishing MedTVT-R1 as a leading solution for complex medical data analysis.

4.3 Qualitative Analysis

MedTVT-R1 demonstrates a robust ability to integrate and analyze data from multiple modalities—CXR, ECG, and LAB tests—to arrive at comprehensive diagnoses. This integration allows for mutual corroboration among the modalities, enhancing diagnostic accuracy, as shown in Figure 4.

- 1) **Multimodal Integration for Diagnosis:** MedTVT-R1 effectively synthesizes information from CXR, ECG, and LAB data to diagnose conditions like hypertension and pneumonia. Each modality provides unique insights that collectively strengthen the diagnostic conclusion. For instance, ECG findings of left ventricular hypertrophy are corroborated by CXR observations of an enlarged cardiac silhouette, both indicative of hypertensive changes. Similarly, LAB results showing elevated white blood cell counts align with CXR evidence of interstitial opacities, supporting a pneumonia diagnosis.
- 2) **Evidence-Based Reasoning:** The model frequently employs terms such as "support," "evident," and "aligns with," highlighting its capability to identify and utilize evidence from each modality to substantiate the final diagnosis. This approach demonstrates MedTVT-R1’s proficiency in extracting relevant features from each dataset, ensuring that the diagnostic reasoning is well-founded and comprehensive. For example, the alignment of elevated pCO₂ and low pH with respiratory compromise underscores the model’s ability to connect LAB findings with CXR results to confirm pneumonia. Overall, MedTVT-R1’s use of multimodal data not only enhances diagnostic precision but also ensures that each diagnosis is supported by a robust evidence base from all available modalities. For more comparisons with the responses of other MLLMs, please refer to the appendix D.

4.4 Ablation Study

The ablation studies in Table 3 clearly demonstrate the effectiveness of both Cyclic Multi-Head Attention (CMHA) and Contribution-Aware Operator (CAO) in the MPL, as well as the necessity of complete modality integration during pre-training. The integration of CMHA and CAO significantly enhances the results, validating our initial intention to design these mechanisms to facilitate modality fusion and adjust the contribution levels of different modalities for various diseases. The presence of all three modalities (ECG, CXR, LAB) results in the best performance. Removing any single modality leads to reduced scores, with the absence of ECG showing the most significant drop in METEOR and ROUGE, possibly because many of the diseases are related to cardiac activity. This underscores the importance of multi-modal integration for optimal outcomes.

5 Conclusion

In conclusion, the proposed MedTVT-R1 framework represents a significant advancement in the application of multimodal large language models (MLLMs) for medical diagnosis. By integrating the complementary strengths of ECG, CXR, and LAB data, MedTVT-R1 addresses the limitations of single-modal approaches and provides a more holistic understanding of complex diseases. The innovative MedTVT-QA dataset facilitates physiological perception and multi-disease diagnosis by leveraging a Chain of Evidence strategy. Additionally, the modality perception layer enhances cross-modal interactions, while Reinforcement Fine-Tuning with Group Relative Policy Optimization and the Jaccard Reward boosts precision and reliability in diagnosis capabilities. Extensive experiments validate MedTVT-R1’s superior performance in both physiological-level understanding and disease-level diagnosis, highlighting its potential for practical clinical applications, such as interpretable diagnostic report generation and complex comorbidity reasoning.

References

- [1] M. Abdelaziz, T. Wang, and A. Elazab. Alzheimer’s disease diagnosis framework from incomplete multimodal data using convolutional neural networks. *Journal of biomedical informatics*, 121:103863, 2021.
- [2] J. Achiam, S. Adler, S. Agarwal, L. Ahmad, I. Akkaya, F. L. Aleman, D. Almeida, J. Altenschmidt, S. Altman, S. Anadkat, et al. Gpt-4 technical report. *arXiv preprint arXiv:2303.08774*, 2023.
- [3] J. M. L. Alcaraz and N. Strodthoff. Cardiolab: Laboratory values estimation and monitoring from electrocardiogram signals—a multimodal deep learning approach. *arXiv preprint arXiv:2411.14886*, 2024.
- [4] Y. Ansari, O. Mourad, K. Qaraqe, and E. Serpedin. Deep learning for ecg arrhythmia detection and classification: an overview of progress for period 2017–2023. *Frontiers in Physiology*, 14:1246746, 2023.
- [5] S. Bai, K. Chen, X. Liu, J. Wang, W. Ge, S. Song, K. Dang, P. Wang, S. Wang, J. Tang, et al. Qwen2. 5-vl technical report. *arXiv preprint arXiv:2502.13923*, 2025.
- [6] A. Bisercic, M. Nikolic, M. van der Schaar, B. Delibasic, P. Lio, and A. Petrovic. Interpretable medical diagnostics with structured data extraction by large language models. *arXiv preprint arXiv:2306.05052*, 2023.
- [7] E. Çalli, E. Sogancioglu, B. van Ginneken, K. G. van Leeuwen, and K. Murphy. Deep learning for chest x-ray analysis: A survey. *Medical image analysis*, 72:102125, 2021.
- [8] A. Cassar, D. R. Holmes Jr, C. S. Rihal, and B. J. Gersh. Chronic coronary artery disease: diagnosis and management. In *Mayo Clinic Proceedings*, volume 84, pages 1130–1146. Elsevier, 2009.
- [9] X. Chen, Y. Niu, J. Fan, L. Lu, and H. Fan. Ecg-based intelligent model for coronary heart disease screening. In *Proceedings of the 2024 11th International Conference on Biomedical and Bioinformatics Engineering*, pages 72–77, 2024.
- [10] A. Dao and D. B. Vu. Alphamaze: Enhancing large language models’ spatial intelligence via grpo. *arXiv preprint arXiv:2502.14669*, 2025.
- [11] M. Deitke, C. Clark, S. Lee, R. Tripathi, Y. Yang, J. S. Park, M. Salehi, N. Muennighoff, K. Lo, L. Soldaini, et al. Molmo and pixmo: Open weights and open data for state-of-the-art multimodal models. *arXiv preprint arXiv:2409.17146*, 2024.
- [12] A. Dosovitskiy, L. Beyer, A. Kolesnikov, D. Weissenborn, X. Zhai, T. Unterthiner, M. Dehghani, M. Minderer, G. Heigold, S. Gelly, et al. An image is worth 16x16 words: Transformers for image recognition at scale. *arXiv preprint arXiv:2010.11929*, 2020.
- [13] A. S. Elstein. On the origins and development of evidence-based medicine and medical decision making. *Inflammation research*, 53:S184–S189, 2004.

- [14] J. Gallifant, M. Afshar, S. Ameen, Y. Aphinyanaphongs, S. Chen, G. Cacciamani, D. Demner-Fushman, D. Dligach, R. Daneshjou, C. Fernandes, et al. The tripod-llm reporting guideline for studies using large language models. *Nature Medicine*, pages 1–10, 2025.
- [15] N. Ghaffar Nia, E. Kaplanoglu, and A. Nasab. Evaluation of artificial intelligence techniques in disease diagnosis and prediction. *Discover Artificial Intelligence*, 3(1):5, 2023.
- [16] B. Gow, T. Pollard, L. A. Nathanson, A. Johnson, B. Moody, C. Fernandes, N. Greenbaum, J. W. Waks, P. Eslami, T. Carbonati, et al. Mimic-iv-ecg: Diagnostic electrocardiogram matched subset. *Type: dataset*, 6:13–14, 2023.
- [17] A. Grattafiori, A. Dubey, A. Jauhri, A. Pandey, A. Kadian, A. Al-Dahle, A. Letman, A. Mathur, A. Schelten, A. Vaughan, et al. The llama 3 herd of models. *arXiv preprint arXiv:2407.21783*, 2024.
- [18] S. Gundapaneni, Z. Zhi, and M. Rodrigues. Deep learning-based noninvasive screening of type 2 diabetes with chest x-ray images and electronic health records. *arXiv preprint arXiv:2412.10955*, 2024.
- [19] D. Guo, D. Yang, H. Zhang, J. Song, R. Zhang, R. Xu, Q. Zhu, S. Ma, P. Wang, X. Bi, et al. Deepseek-r1: Incentivizing reasoning capability in llms via reinforcement learning. *arXiv preprint arXiv:2501.12948*, 2025.
- [20] M. Hernandez, G. Epelde, A. Alberdi, R. Cilla, and D. Rankin. Synthetic data generation for tabular health records: A systematic review. *Neurocomputing*, 493:28–45, 2022.
- [21] E. J. Hu, Y. Shen, P. Wallis, Z. Allen-Zhu, Y. Li, S. Wang, L. Wang, W. Chen, et al. Lora: Low-rank adaptation of large language models. *ICLR*, 1(2):3, 2022.
- [22] J. Huang, D. M. Yang, R. Rong, K. Nezafati, C. Treager, Z. Chi, S. Wang, X. Cheng, Y. Guo, L. J. Klesse, et al. A critical assessment of using chatgpt for extracting structured data from clinical notes. *npj Digital Medicine*, 7(1):106, 2024.
- [23] J. Irvin, P. Rajpurkar, M. Ko, Y. Yu, S. Ciurea-Ilcus, C. Chute, H. Marklund, B. Haghighi, R. Ball, K. Shpanskaya, et al. Chexpert: A large chest radiograph dataset with uncertainty labels and expert comparison. In *Proceedings of the AAAI conference on artificial intelligence*, volume 33, pages 590–597, 2019.
- [24] M. Jin, Q. Yu, C. Zhang, D. Shu, S. Zhu, M. Du, Y. Zhang, and Y. Meng. Health-llm: Personalized retrieval-augmented disease prediction model. *arXiv preprint arXiv:2402.00746*, 10, 2024.
- [25] A. Johnson, L. Bulgarelli, T. Pollard, S. Horng, L. A. Celi, and R. Mark. Mimic-iv. *PhysioNet*. Available online at: <https://physionet.org/content/mimiciv/1.0/>(accessed August 23, 2021), pages 49–55, 2020.
- [26] A. E. Johnson, T. J. Pollard, N. R. Greenbaum, M. P. Lungren, C.-y. Deng, Y. Peng, Z. Lu, R. G. Mark, S. J. Berkowitz, and S. Horng. Mimic-cxr-jpg, a large publicly available database of labeled chest radiographs. *arXiv preprint arXiv:1901.07042*, 2019.
- [27] A. Kline, H. Wang, Y. Li, S. Dennis, M. Hutch, Z. Xu, F. Wang, F. Cheng, and Y. Luo. Multimodal machine learning in precision health: A scoping review. *npj Digital Medicine*, 5(1):171, 2022.
- [28] A. Kumar. Deep learning for multi-modal medical imaging fusion: Enhancing diagnostic accuracy in complex disease detection. *Int J Eng Technol Res Manag*, 6(11):183, 2022.
- [29] Y. Lai, J. Zhong, M. Li, S. Zhao, and X. Yang. Med-r1: Reinforcement learning for generalizable medical reasoning in vision-language models. *arXiv preprint arXiv:2503.13939*, 2025.
- [30] X. Lan, F. Wu, K. He, Q. Zhao, S. Hong, and M. Feng. Gem: Empowering mllm for grounded ecg understanding with time series and images. *arXiv preprint arXiv:2503.06073*, 2025.
- [31] S. Lee, W. J. Kim, J. Chang, and J. C. Ye. Llm-cxr: instruction-finetuned llm for cxr image understanding and generation. *arXiv preprint arXiv:2305.11490*, 2023.

- [32] S. Lee, J. Youn, H. Kim, M. Kim, and S. H. Yoon. Cxr-llava: a multimodal large language model for interpreting chest x-ray images. *European Radiology*, pages 1–13, 2025.
- [33] B. Li, K. Zhang, H. Zhang, D. Guo, R. Zhang, F. Li, Y. Zhang, Z. Liu, and C. Li. Llava-next: Stronger llms supercharge multimodal capabilities in the wild, May 2024.
- [34] B. Li, Y. Zhang, D. Guo, R. Zhang, F. Li, H. Zhang, K. Zhang, P. Zhang, Y. Li, Z. Liu, et al. Llava-onevision: Easy visual task transfer. *arXiv preprint arXiv:2408.03326*, 2024.
- [35] C. Li, C. Wong, S. Zhang, N. Usuyama, H. Liu, J. Yang, T. Naumann, H. Poon, and J. Gao. Llava-med: Training a large language-and-vision assistant for biomedicine in one day. *Advances in Neural Information Processing Systems*, 36:28541–28564, 2023.
- [36] C.-Y. Li, K.-J. Chang, C.-F. Yang, H.-Y. Wu, W. Chen, H. Bansal, L. Chen, Y.-P. Yang, Y.-C. Chen, S.-P. Chen, et al. Towards a holistic framework for multimodal llm in 3d brain ct radiology report generation. *Nature Communications*, 16(1):2258, 2025.
- [37] V. Liévin, C. E. Hother, A. G. Motzfeldt, and O. Winther. Can large language models reason about medical questions? *Patterns*, 5(3), 2024.
- [38] C.-S. Lin, Y.-T. Lee, W.-H. Fang, Y.-S. Lou, F.-C. Kuo, C.-C. Lee, and C. Lin. Deep learning algorithm for management of diabetes mellitus via electrocardiogram-based glycosylated hemoglobin (ecg-hba1c): a retrospective cohort study. *Journal of Personalized Medicine*, 11(8):725, 2021.
- [39] C. Liu, Y. Tian, W. Chen, Y. Song, and Y. Zhang. Bootstrapping large language models for radiology report generation. In *Proceedings of the AAAI Conference on Artificial Intelligence*, volume 38, pages 18635–18643, 2024.
- [40] H. Liu, C. Li, Y. Li, and Y. J. Lee. Improved baselines with visual instruction tuning. In *Proceedings of the IEEE/CVF Conference on Computer Vision and Pattern Recognition*, pages 26296–26306, 2024.
- [41] H. Liu, C. Li, Q. Wu, and Y. J. Lee. Visual instruction tuning. *Advances in neural information processing systems*, 36:34892–34916, 2023.
- [42] S. Liu, A. S. Hussain, Q. Wu, C. Sun, and Y. Shan. Mumu-llama: Multi-modal music understanding and generation via large language models. *arXiv preprint arXiv:2412.06660*, 2024.
- [43] X. Liu, H. Wang, Z. Li, and L. Qin. Deep learning in ecg diagnosis: A review. *Knowledge-Based Systems*, 227:107187, 2021.
- [44] Z. Liu, Z. Sun, Y. Zang, X. Dong, Y. Cao, H. Duan, D. Lin, and J. Wang. Visual-rft: Visual reinforcement fine-tuning. *arXiv preprint arXiv:2503.01785*, 2025.
- [45] H. Lu, W. Liu, B. Zhang, B. Wang, K. Dong, B. Liu, J. Sun, T. Ren, Z. Li, H. Yang, et al. Deepseek-vl: towards real-world vision-language understanding. *arXiv preprint arXiv:2403.05525*, 2024.
- [46] M. Y. Lu, B. Chen, D. F. Williamson, R. J. Chen, M. Zhao, A. K. Chow, K. Ikemura, A. Kim, D. Pouli, A. Patel, et al. A multimodal generative ai copilot for human pathology. *Nature*, 634(8033):466–473, 2024.
- [47] J. Pan, C. Liu, J. Wu, F. Liu, J. Zhu, H. B. Li, C. Chen, C. Ouyang, and D. Rueckert. Medvlm-r1: Incentivizing medical reasoning capability of vision-language models (vlms) via reinforcement learning. *arXiv preprint arXiv:2502.19634*, 2025.
- [48] S. S. Ramesh, Y. Hu, I. Chaimalas, V. Mehta, P. G. Sessa, H. Bou Ammar, and I. Bogunovic. Group robust preference optimization in reward-free rlhf. *Advances in Neural Information Processing Systems*, 37:37100–37137, 2024.
- [49] A. Saporta, A. M. Puli, M. Goldstein, and R. Ranganath. Contrasting with symple: Simple model-agnostic representation learning for unlimited modalities. *Advances in Neural Information Processing Systems*, 37:56919–56957, 2024.

- [50] J. Schulman, F. Wolski, P. Dhariwal, A. Radford, and O. Klimov. Proximal policy optimization algorithms. *arXiv preprint arXiv:1707.06347*, 2017.
- [51] Z. Shao, P. Wang, Q. Zhu, R. Xu, J. Song, X. Bi, H. Zhang, M. Zhang, Y. Li, Y. Wu, et al. Deepseekmath: Pushing the limits of mathematical reasoning in open language models. *arXiv preprint arXiv:2402.03300*, 2024.
- [52] J. Shentu and N. Al Moubayed. Cxr-irgen: an integrated vision and language model for the generation of clinically accurate chest x-ray image-report pairs. In *Proceedings of the IEEE/CVF Winter Conference on Applications of Computer Vision*, pages 5212–5221, 2024.
- [53] S. Steyaert, M. Pizurica, D. Nagaraj, P. Khandelwal, T. Hernandez-Boussard, A. J. Gentles, and O. Gevaert. Multimodal data fusion for cancer biomarker discovery with deep learning. *Nature machine intelligence*, 5(4):351–362, 2023.
- [54] N. Strodthoff, J. M. Lopez Alcaraz, and W. Haverkamp. Mimic-iv-ecg-ext-icd: Diagnostic labels for mimic-iv-ecg (version 1.0.1). *PhysioNet*, 2024.
- [55] M. S. I. Sumon, M. S. B. Islam, M. S. Rahman, M. S. A. Hossain, A. Khandakar, A. Hasan, M. Murugappan, and M. E. Chowdhury. Cardiotabnet: A novel hybrid transformer model for heart disease prediction using tabular medical data. *arXiv preprint arXiv:2503.17664*, 2025.
- [56] H. Tan, Y. Ji, X. Hao, M. Lin, P. Wang, Z. Wang, and S. Zhang. Reason-rft: Reinforcement fine-tuning for visual reasoning. *arXiv preprint arXiv:2503.20752*, 2025.
- [57] R. Tanno, D. G. Barrett, A. Sellergren, S. Ghaisas, S. Dathathri, A. See, J. Welbl, C. Lau, T. Tu, S. Azizi, et al. Collaboration between clinicians and vision–language models in radiology report generation. *Nature Medicine*, 31(2):599–608, 2025.
- [58] Y. Tian, Z. Li, Y. Jin, M. Wang, X. Wei, L. Zhao, Y. Liu, J. Liu, and C. Liu. Foundation model of ecg diagnosis: Diagnostics and explanations of any form and rhythm on ecg. *Cell Reports Medicine*, 5(12), 2024.
- [59] Z. Tian, Y. Jin, Z. Liu, R. Yuan, X. Tan, Q. Chen, W. Xue, and Y. Guo. Audiox: Diffusion transformer for anything-to-audio generation. *arXiv preprint arXiv:2503.10522*, 2025.
- [60] J. Venugopalan, L. Tong, H. R. Hassanzadeh, and M. D. Wang. Multimodal deep learning models for early detection of alzheimer’s disease stage. *Scientific reports*, 11(1):3254, 2021.
- [61] S. Wu, H. Fei, L. Qu, W. Ji, and T.-S. Chua. Next-gpt: Any-to-any multimodal llm. In *Forty-first International Conference on Machine Learning*, 2024.
- [62] K. Yang, M. Hong, J. Zhang, Y. Luo, S. Zhao, O. Zhang, X. Yu, J. Zhou, L. Yang, P. Zhang, et al. Ecg-llm: Understanding electrocardiogram with a large language model. *Health Data Science*, 5:0221, 2025.
- [63] W. Yao, C. Liu, K. Yin, W. Cheung, and J. Qin. Addressing asynchronicity in clinical multimodal fusion via individualized chest x-ray generation. *Advances in Neural Information Processing Systems*, 37:29001–29028, 2024.
- [64] C. Yu, A. Velu, E. Vinitzky, J. Gao, Y. Wang, A. Bayen, and Y. Wu. The surprising effectiveness of ppo in cooperative multi-agent games. *Advances in neural information processing systems*, 35:24611–24624, 2022.
- [65] H. Yu, P. Guo, and A. Sano. Zero-shot ecg diagnosis with large language models and retrieval-augmented generation. In *Machine learning for health (ML4H)*, pages 650–663. PMLR, 2023.
- [66] D. Yuan, E. Rastogi, G. Naik, S. P. Rajagopal, S. Goyal, F. Zhao, B. Chintagunta, and J. Ward. A continued pretrained llm approach for automatic medical note generation. *arXiv preprint arXiv:2403.09057*, 2024.
- [67] H. Zhang, X. Li, and L. Bing. Video-llama: An instruction-tuned audio-visual language model for video understanding. *arXiv preprint arXiv:2306.02858*, 2023.

- [68] Y. Zhao, J. Huang, J. Hu, X. Wang, Y. Mao, D. Zhang, Z. Jiang, Z. Wu, B. Ai, A. Wang, et al. Swift: a scalable lightweight infrastructure for fine-tuning. In *Proceedings of the AAAI Conference on Artificial Intelligence*, volume 39, pages 29733–29735, 2025.
- [69] Y. Zhao, T. Zhang, X. Wang, P. Han, T. Chen, L. Huang, Y. Jin, and J. Kang. Ecg-chat: A large ecg-language model for cardiac disease diagnosis. *arXiv preprint arXiv:2408.08849*, 2024.
- [70] J. Zhu, W. Wang, Z. Chen, Z. Liu, S. Ye, L. Gu, Y. Duan, H. Tian, W. Su, J. Shao, et al. Internvl3: Exploring advanced training and test-time recipes for open-source multimodal models. *arXiv preprint arXiv:2504.10479*, 2025.

A Details About the Prompts of MedTVT-QA’s Construction

This section presents the detailed prompts used in constructing the MedTVT-QA dataset.

ECG-QA Prompt

Role Setting: You are a renowned cardiologist with expertise in interpreting electrocardiograms (ECGs).

Task Description: The ECG analysis has yielded the following labels: {labels}. Based on these labels, please address the question: {question}.

Answer Guidance: Your response should incorporate all relevant labels, excluding any unrelated ones. Provide a synthesis of the labels, focusing on clinical significance.

Answer Format: Begin with a brief introduction to your analysis. Provide detailed explanations for each specific ECG label. Offer a concise summary.

CXR-QA Prompt

Role Setting: You are a radiology expert with expertise in interpreting chest X-ray image.

Task Description: The chest X-ray report is given {report}. Base on the given chest X-ray report, answer the question {question}.
Answer Guidance: Describe the overall condition of the lungs, heart, and chest cavity in the image. Identify and explain any abnormal findings such as shadows, opacities, effusions, or masses. Provide possible diagnoses.

LAB-QA Prompt

Role Setting: Please analyze this set of blood test data as a medical professional.

Task Description: This is the question: {question}. The following are the lab data: "Hematocrit": {data[0]}; "Platelet Count": {data[1]}; "Creatinine": {data[2]}; "Potassium": {data[3]}; "Hemoglobin": {data[4]}; "White Blood Cells": {data[5]}; "MCHC": {data[6]}; "Red Blood Cells": {data[7]}; "MCV": {data[8]}; "MCH": {data[9]}; "RDW": {data[10]}; "Urea Nitrogen": {data[11]}; "Sodium": {data[12]}; "Chloride": {data[13]}; "Bicarbonate": {data[14]}; "Anion Gap": {data[15]}; "Glucose": {data[16]}; "Magnesium": {data[17]}; "Calcium, Total": {data[18]}; "Phosphate": {data[19]}; "INR(PT)": {data[20]}; "PT": {data[21]}; "PTT": {data[22]}; "Basophils": {data[23]}; "Neutrophils": {data[24]}; "Monocytes": {data[25]}; "Eosinophils": {data[26]}; "Lymphocytes": {data[27]}; "RDW-SD": {data[28]}; "H": {data[29]}; "L": {data[30]}; "I": {data[31]}; "Alanine Aminotransferase (ALT)": {data[32]}; "Aspartate Aminotransferase (AST)": {data[33]}; "Lactate": {data[34]}; "Alkaline Phosphatase": {data[35]}; "Bilirubin, Total": {data[36]}; "pH": {data[37]}; "Albumin": {data[38]}; "Base Excess": {data[39]}; "pO2": {data[40]}; "Calculated Total CO2": {data[41]}; "pCO2": {data[42]}; "Absolute Neutrophil Count": {data[43]}; "Absolute Eosinophil Count": {data[44]}; "Absolute Monocyte Count": {data[45]}; "Absolute Basophil Count": {data[46]}; "Absolute Lymphocyte Count": {data[47]}; "Creatine Kinase (CK)": {data[48]}; "Immature Granulocytes": {data[49]}.

Answer Guidance: These data comprise 50 different indicators, categorized into seven main classes: routine blood indicators, electrolyte and metabolic indicators, renal function indicators, liver function indicators, acid-base balance and gas exchange, coagulation function indicators, and other indicators.

Answer Format: Begin with a brief introduction to your analysis.

routine blood indicators: explanation

electrolyte and metabolic indicators: explanation

renal function indicators: explanation

liver function indicators: explanation

acid-base balance and gas exchange: explanation

coagulation function indicators: explanation

other indicators: explanation

Finally, offer a concise summary.

Disease-QA Prompt

Role Setting: You are a renowned diagnostician with expertise in integrating ECG, CXR, and blood test results.

Task Description: The following diagnostics have been provided:

- ECG Analysis: {ecg_report}
- CXR Analysis: {cxr_report}
- Blood Test Analysis: {blood_test_report}
- Diseases: {result_diseases}

You need to pretend that the ECG, CXR, and blood test analyses are based on your interpretation of the raw data, and the final diagnosis is your synthesis of these three diagnostic methods, please address the question: {question}.

Answer Guidance: Please find definitive evidence from the ECG, CXR, and blood test results, leveraging the complementarity and mutual corroboration of these three modalities, to robustly prove the reasons why the patient has the diseases I provided. Your response must include every disease I provided, using the exact wording I provided, and you must not mention any diseases other than those I provided. Please make sure to provide evidence for these diagnoses! These are confirmed conditions.

Answer Format: <think>[Diagnostic evidence synthesized from the three modalities]</think>\n <answer>{disease1; disease2; ...}</answer>

B Label Distribution of MedTVT-QA

When constructing the physiology-level ECG-QA dataset, we filtered out invalid ECG labels to ensure that the final labels align with morphology descriptions at the physiological level. Additionally, we conducted a detailed statistical analysis of the labels in the ECG-QA training data. As shown in Table 4, it presents ECG labels with occurrences greater than 100 along with their respective counts.

Table 4: ECG Labels and Counts (>100) in ECG-QA.

Label	Count
sinus rhythm with 1st degree a-v block	140
sinus rhythm	4033
atrial fibrillation	761
sinus tachycardia	1565
consider acute st elevation mi	161
atrial fibrillation with rapid ventricular response	224
age not entered, assumed to be 50 years old for purpose of ecg interpretation	328
sinus bradycardia	402
sinus rhythm with pac(s)	132
sinus rhythm with borderline 1st degree a-v block	121
pacemaker rhythm - no further analysis	160
leftward axis	435
possible left anterior fascicular block	138
rightward axis	164
probable left atrial enlargement	224
low qrs voltages in precordial leads	540
st junctional depression is nonspecific	149
possible inferior infarct - age undetermined	425
lateral t wave changes are nonspecific	328
short pr interval	167
inferior t wave changes are nonspecific	312
left ventricular hypertrophy	428
lvh with secondary repolarization abnormality	285
left axis deviation	1067
poor r wave progression - probable normal variant	538
indeterminate axis	108
possible anterior infarct - age undetermined	511
anterior t wave changes are nonspecific	182
possible left atrial abnormality	271
inferior/lateral st-t changes are nonspecific	240
prolonged qt interval	618
possible anteroseptal infarct - age undetermined	254
septal t wave changes are nonspecific	134
right bundle branch block	517
lateral st-t changes are nonspecific	289
anteroseptal infarct - age undetermined	129
left anterior fascicular block	202
extensive st-t changes are nonspecific	111
inferior infarct - age undetermined	550
rsr'(v1) - probable normal variant	199
left bundle branch block	354
low qrs voltages in limb leads	395
extensive st-t changes may be due to myocardial ischemia	143
possible left ventricular hypertrophy	150
abnormal r-wave progression, early transition	102
inferior infarct, old	123
ventricular premature complex	119
possible septal infarct - age undetermined	188
right axis deviation	141
lateral st-t changes may be due to myocardial ischemia	227
inferior/lateral st-t changes may be due to myocardial ischemia	167
iv conduction defect	376
generalized low qrs voltages	161
qrs changes v3/v4 may be due to lvh but cannot rule out anterior infarct	103

Label	Count
lateral t wave changes may be due to myocardial ischemia	106
rbbb with left anterior fascicular block	314
extensive st-t changes may be due to hypertrophy and/or ischemia	135
normal ecg	753
normal ecg except for rate	334
abnormal ecg	4761
borderline ecg	2074
inferior/lateral st-t changes may be due to hypertrophy and/or ischemia	116
lateral st-t changes may be due to hypertrophy and/or ischemia	112

Figure 5 presents an example report from the MIMIC-IV-CXR dataset, used in constructing CXR-QA. The report contains some unclear and unrelated content to the CXR image description. By applying the previously described CXR prompts, we transformed the report into a more organized and focused description centered on CXR.

Figure 5: An CXR report example from MIMIX-IV-CXR-report dataset.

FINAL REPORT
<p>EXAMINATION: CHEST (PA AND LAT)</p> <p>INDICATION: ___F with new onset ascites // eval for infection</p> <p>TECHNIQUE: Chest PA and lateral</p> <p>COMPARISON: None.</p> <p>FINDINGS: There is no focal consolidation, pleural effusion or pneumothorax. Bilateral nodular opacities that most likely represent nipple shadows. The cardiomeastinal silhouette is normal. Clips project over the left lung, potentially within the breast. The imaged upper abdomen is unremarkable. Chronic deformity of the posterior left sixth and seventh ribs are noted.</p> <p>IMPRESSION: No acute cardiopulmonary process.</p>

Disease-level labels are derived from the MIMIC-IV-ECG-EXT-ICD [54] dataset, with these labels stored as ICD-10 codes. Each sample may correspond to multiple disease categories. We filtered out diseases for which evidence could not be found in ECG, CXR, or LAB data. Ultimately, we identified seven main categories: Coronary Artery Disease, Acute Renal Failure, Hypertension, Atrial Fibrillation, Pneumonia, Diabetes Mellitus, and Sepsis, along with some subclasses within these categories. Details are provided in Table 5.

Table 5: ICD-10 Disease Statistics with Corresponding Counts.

Disease Category	ICD-10 Code	Count
Coronary Artery Disease		
Coronary Artery Disease	I2510	2680
Chronic ischemic heart disease, unspecified	I252	936
Atherosclerotic heart disease of native coronary artery	I259	190
Other forms of chronic ischemic heart disease	I253	8
Ischemic cardiomyopathy	I255	79
Acute Renal Failure		
Acute kidney failure, unspecified	N179	2379
Acute kidney failure with tubular necrosis	N170	689
Acute kidney failure with other specified morphologic lesions	N178	12
Acute kidney failure with acute cortical necrosis	N171	1
Hypertension		
Essential (primary) hypertension	I10	4155
Hypertensive heart and chronic kidney disease, unspecified	I129	1536
Hypertensive heart disease with heart failure	I120	515
Hypertensive heart and chronic kidney disease with heart failure	I130	119
Hypertensive heart disease without heart failure	I110	77
Hypertensive heart and chronic kidney disease with heart failure and stage 5 CKD or ESRD	I132	37
Hypertensive heart disease, unspecified	I119	8
Other secondary hypertension	I159	1
Renovascular hypertension	I150	7
Other specified secondary hypertension	I158	1
Atrial Fibrillation		
Persistent atrial fibrillation	I4891	2623
Permanent atrial fibrillation	I4892	317
Paroxysmal atrial fibrillation	I480	237
Other specified atrial fibrillation	I482	104
Atrial flutter, unspecified	I481	15
Typical atrial flutter	I483	1
Atypical atrial flutter	I484	1
Pneumonia		

Disease Category	ICD-10 Code	Count
Pneumonia, unspecified organism	J189	1442
Pneumonia due to other specified bacteria	J181	25
Pneumonia due to Haemophilus influenzae	J188	18
Pneumonia due to Klebsiella pneumoniae	J180	5
Diabetes Mellitus		
Type 2 diabetes mellitus without complications	E119	1752
Type 2 diabetes mellitus with unspecified complications	E1129	217
Type 2 diabetes mellitus with hyperglycemia	E11319	296
Type 2 diabetes mellitus with renal complications	E1140	348
Type 2 diabetes mellitus with circulatory complications	E1165	360
Type 2 diabetes mellitus with other specified complications	E118	29
Type 2 diabetes mellitus with unspecified complications	E139	29
Type 1 diabetes mellitus without complications	E109	27
Type 1 diabetes mellitus with unspecified complications	E138	2
Type 1 diabetes mellitus with other specified complications	E108	3
Sepsis		
Sepsis, unspecified organism	A419	1088
Severe sepsis without septic shock	R6520	939
Severe sepsis with septic shock	R6521	873
Sepsis due to Streptococcus pneumoniae	A403	26
Sepsis due to Escherichia coli	A412	2
Sepsis due to other Gram-negative organisms	A409	69
Sepsis due to anaerobes	A414	28
Sepsis due to other specified bacteria	A411	26
Sepsis due to Staphylococcus aureus	A401	3
Sepsis due to other specified Staphylococcus	A408	4
Sepsis due to other specified bacteria	A413	1
Sepsis due to unspecified Staphylococcus	A400	2

C Examples of QA Pairs Corresponding to Each Modality

This section provides examples of question-answer pairs corresponding to each modality (e.g., ECG, CXR, LAB) in the MedTVT-QA dataset.

ECG-QA Example

Question: What information can be derived from the ECG <ecg>?

Answer: ECG Analysis: Upon evaluating the electrocardiogram (ECG), the following observations can be made:

1. Sinus Rhythm: The heart is under the control of the sinoatrial (SA) node, which is the natural pacemaker. This finding suggests that the electrical activity of the heart is originating from the SA node and progressing through the normal conduction pathway, leading to a regular rhythm. This is a foundational indicator of organized cardiac activity.

2. Left Bundle Branch Block (LBBB): There is evidence of delayed or disrupted conduction through the left bundle of the heart's electrical conduction system. This results in a characteristic pattern on the ECG, with a widened QRS complex (>120 ms) and specific morphologies in leads, such as a broad, notched appearance in V5-V6 and an absence of normal septal depolarization. LBBB may occur in conditions like ischemic heart disease, cardiomyopathy, or hypertension-induced structural changes, though it can also occasionally be found in asymptomatic individuals.

Summary: The heart demonstrates a sinus rhythm, indicating normal initiation of electrical activity. However, the presence of a left bundle branch block signifies an abnormality in electrical conduction, often associated with underlying cardiac pathology. As a whole, this ECG is classified as abnormal due to the conduction disturbance, warranting further investigation to assess structural or functional cardiac issues.

CXR-QA Example

Question: Would you mind explaining the findings on my chest X-ray <cxr>?

Answer: Based on the evaluation of your chest X-ray image, the lungs appear overall unchanged from prior assessments, indicating no new substantial developments. There is no evidence of acute cardiopulmonary disease, which means there are no significant new concerns regarding your heart or lungs. Specifically, there are no signs of pneumonia, which would typically appear as clouded or consolidated areas in the lung fields. Similarly, there is no vascular congestion; this would generally be associated with heart-related problems affecting the lung's blood vessels and is absent in this image. Additionally, there is no pleural effusion, which would be fluid accumulation in the space between the lungs and chest wall.

However, there is a notable finding of a dense streak of atelectasis at the left base of the lung, which is a condition where a part of the lung collapses or does not inflate properly, resulting in that portion not being fully functional. This streak appears denser than usual tissue, indicating that a segment of the lung at the left base may not be fully expanded or aerated. Atelectasis can result from various causes, such as mucus blocking an airway, external pressure on the lung, or post-surgical changes.

Despite this abnormality, the absence of acute cardiopulmonary disease indicators is reassuring. The streak of atelectasis should be monitored, and clinical correlation with your symptoms is important. Continuous observation or additional imaging might be recommended to ensure there are no underlying issues contributing to this finding. Always consult with your healthcare provider to discuss the implications of these findings based on your clinical history and symptoms.

LAB-QA Example

Question: Would you be able to undertake a comprehensive examination of this patient’s blood panel <lab>, including the reference ranges and clinical implications associated with all abnormal values?

Answer: Comprehensive Blood Panel Analysis: This blood test reflects multiple systemic functions. I will analyze the provided values across seven categories, indicating normal findings and clinical implications for abnormal or missing data.

Routine Blood Indicators: Hematocrit, hemoglobin, red blood cells, MCV, and MCHC fall within normal ranges, suggesting typical oxygen-carrying capacity and erythrocyte health. RDW is borderline high, which could indicate subtle variability in red cell size, potentially pointing toward early nutritional deficiencies or mild anemia. Platelet count and white blood cells are normal, showing adequate clotting potential and immune activity. All differential leukocyte percentages are within normal ranges, reflecting balanced immunity.

Electrolyte and Metabolic Indicators: Potassium, sodium, magnesium, bicarbonate, and phosphate are within normal ranges, indicating balanced electrolytes and acid-base homeostasis. However, chloride is mildly low (97.0), potentially reflecting minor electrolyte imbalance or compensatory metabolic alkalosis. Glucose is significantly elevated (185.0), possibly suggesting poorly controlled diabetes mellitus or acute hyperglycemia. Lactate is elevated (4.6), which could suggest tissue hypoxia or metabolic distress. Calcium is borderline low (8.5), potentially indicating subtle hypocalcemia warranting further evaluation.

Renal Function Indicators: Creatinine is within the high-normal range, which might raise concerns for early renal insufficiency depending on age/gender. Urea nitrogen is elevated, possibly indicating dehydration, increased protein metabolism, or mild renal dysfunction.

Liver Function Indicators: ALT, AST, bilirubin, and alkaline phosphatase values are missing and assumed normal, precluding further analysis.

Acid-Base Balance and Gas Exchange: With missing pH and gas exchange values, bicarbonate is normal but anion gap is elevated (22.0), potentially indicating metabolic acidosis from lactate accumulation or unmeasured ions.

Coagulation Function Indicators: INR, PT, and PTT are missing and presumed normal, suggesting no overt coagulation abnormalities.

Other Indicators: Data gaps in albumin, base excess, and other parameters limit full metabolic insight.

Summary: Elevated glucose and lactate suggest metabolic dysregulation. Elevated urea nitrogen and borderline creatinine warrant renal assessment. Mild hypocalcemia and low chloride need further exploration. Elevated anion gap hints at underlying acidosis. Follow-up tests are recommended for confirmation and diagnosis refinement.

D Performance of Various MLLMs in Handling Medical Reasoning and Diagnosis

Here, we present an example of medical analysis and diagnosis among various MLLMs and MedTVT-R1, as shown in Figure 6.

E Limitation

Although our proposed MedTVT-R1 successfully integrates CXR, ECG, and LAB data for joint multi-disease diagnosis, there are still some limitations. First, precise disease diagnosis often requires a larger volume of multimodal data collected from the same patient within a similar timeframe. However, in the short term, it is challenging to gather such large-scale data, which limits the model’s generalization ability and diagnostic accuracy. Second, while our work incorporates three modalities—CXR, ECG, and LAB—more accurate disease analysis and diagnosis may rely on additional modalities, such as patient medical history, genomic data, or other biomarkers. Unfortunately, the current open-source datasets lack richer multimodal information, making such extensions difficult to achieve. Future research could aim to address these challenges to further enhance the model’s diagnostic capabilities and practical applicability.

	What illnesses might be indicated by the findings from my ECG <ecg>, CXR <cxr>, and blood work <lab>?
MedTVT-R1	<p><think>Based on the ECG, CXR, and blood test analyses, the findings collectively support the presence of Diabetes Mellitus and Hypertension. The diagnosis of Diabetes Mellitus is substantiated by blood test results. The markedly elevated glucose levels indicate hyperglycemia, a hallmark of diabetes. Although this blood test result suggests persistent elevated glucose levels, acute complications such as low glucose levels are characteristic of diabetes. Additionally, mild anemia and low albumin could reflect chronic disease-related nutritional deficits or underlying inflammatory processes often associated with diabetes. The low-normal albumin level may further suggest chronic systemic effects often seen in diabetes-related complications.</p> <p>The diagnosis of Hypertension is supported by findings from all three diagnostic modalities. The ECG demonstrates a sinus rhythm with borderline findings, which can be associated with increased cardiac workload often seen in hypertensive patients. The presence of a small left-sided pleural effusion and mild pulmonary edema on the CXR aligns with fluid retention often seen in hypertensive heart disease or postoperative states. While the heart size is not detailed here, the pleural effusions seen on imaging may indirectly support hypertensive fluid shifts or cardiovascular strain. Elevated creatinine and urea nitrogen on the blood test suggest possible hypertensive nephropathy or reduced renal filtration rates. Hyperglycemia may further exacerbate vascular strain linked to hypertension.</p> <p>In conclusion, the evidence points to Diabetes Mellitus through hyperglycemia, and Hypertension through cardiac strain and renal involvement clearly through indirect ECG and CXR findings. Both conditions require further management to mitigate systemic and cardiovascular risks.</think></p> <p><answer>Diabetes Mellitus; Hypertension</answer></p>
Qwen2.5-VL-3B-Instruct	<p>The provided ECG and chest X-ray images can be analyzed together to identify potential health issues. Here's a step-by-step analysis:</p> <p>ECG Analysis: 1. P Waves: The P waves appear normal in all leads (I, II, III, aVR, aVL, aVF, V1-V6). This suggests that the atrial activity is normal. 2. QRS Complexes: The QRS complexes are wide and have a duration of approximately 120ms, which is indicative of left ventricular hypertrophy (LVH). 3. T Waves: The T waves are not significantly abnormal in any lead. 4. ST Segments: The ST segments are within normal limits.</p> <p>Chest X-Ray Analysis:</p> <ol style="list-style-type: none"> Cardiac Size: The cardiac silhouette appears enlarged, which could be due to LVH or other cardiomegaly causes. Lung Fields: The lung fields appear clear with no signs of consolidation, effusion, or other abnormalities. Heart Position: The heart position is normal, with no evidence of cardiomegaly or pericardial effusion. <p>Blood Test Results:</p> <p>Creatinine: 0.2264026403427124 mg/dL (normal range: 0.6–1.2 mg/dL) BUN: 0.2870349884033203 mg/dL (normal range: 7–20 mg/dL) Calcium: 0.6595468521118164 mg/dL (normal range: 8.5–10.5 mg/dL) Magnesium: 0.345366507768631 mg/dL (normal range: 1.7–2.6 mg/dL) Potassium: 0.4424666166305542mEq/L (normal range: 3.5–5.0mEq/L) Sodium: 0.524380087852478mEq/L (normal range: 135–145 mEq/L) Chloride: 0.5399884581</p>
InternVL3-1B	<p>Based on the ECG and chest X-ray provided, the possible health concerns could include:</p> <ol style="list-style-type: none"> Arrhythmias: These include abnormal heart rhythms such as bradycardia, tachycardia, or atrial fibrillation, indicated by the presence of irregular QRS complexes. Cardiomyopathy: Structural changes in the heart muscle, which might be visible on the ECG with abnormal heart rhythm patterns. Valvular Aortic Stenosis: The semi-erect portable chest X-ray suggests possible pulmonary hypertension as the vascular structures seen suggest dilation in pulmonary valve and possibly aortic root shadow suggesting valve involvement. Coronary Artery Disease: Though less likely in this chest X-ray alone, subtle changes could indicate coronary artery disease. Electrolyte Imbalance: Such as hyperkalemia, which could be visible on an abnormal heart rhythm from changes in heart rhythm patterns. <p>These are general possibilities and specific diagnoses would need further clinical evaluation and possibly additional investigations such as Holter monitoring, CT angiography, a cardiac MRI, or a stress test.</p>
LLaVA-One-Vision-7B	<p>The image you've provided appears to show medical test results and an X-ray. However, since I am an AI and not a licensed medical professional, I cannot diagnose or provide a medical opinion based on these images. If you are concerned about your health or test results, you should consult with a licensed healthcare provider for a proper interpretation and advice. They would be able to evaluate the test results and the associated X-ray in the context of your symptoms and medical history, which is essential for an accurate diagnosis.</p>
Ground-Truth	<p><think>Based on the integrated analysis of the ECG, chest X-ray (CXR), and blood test results, the findings align with the provided diagnoses of Diabetes Mellitus and Hypertension.</p> <p>Diabetes Mellitus: The elevated blood glucose level, while not definitively diagnostic on its own, suggests potential impaired fasting glucose. This could indicate underlying diabetes or prediabetes, particularly in the absence of detailed glucose tolerance or HbA1c data. Additionally, the mild metabolic acidosis evidenced by the low bicarbonate and elevated anion gap may point to incomplete buffering of acids, a finding consistent with diabetic ketoacidosis in uncontrolled diabetes. Though no renal dysfunction is apparent, the possibility of early metabolic derangements related to diabetes warrants consideration given these findings.</p> <p>Hypertension: While the ECG reveals a sinus rhythm with no overt electrical abnormalities, prolonged hypertension can result in adverse structural or functional changes not immediately evident on ECG. However, CXR findings suggest some correlation with hypertensive pathology. The stable heart and mediastinal contours, coupled with the noted small left pleural effusion, may reflect subtle signs of longstanding hypertension potentially leading to vascular or cardiac strain over time. Additionally, the subtle branching opacities in the right lower lobe may represent congestion secondary to hypertensive changes, though more definitive evidence of heart failure is absent. Furthermore, the normal kidney-related parameters (creatinine, urea nitrogen) on the blood test suggest preserved renal function, which is crucial in chronic hypertension management.</p> <p>In summary, elevated glucose and metabolic abnormalities strongly support Diabetes Mellitus, while combined CXR and blood test data suggest secondary effects or subtle complications associated with Hypertension. Careful monitoring and targeted interventions for both conditions are warranted.</think></p> <p><answer>Diabetes Mellitus; Hypertension</answer></p>

Figure 6: Performance of various MLLMs in handling medical reasoning and diagnosis. MedTVT-R1 approaches from the perspective of illness, tracing and identifying evidence of related diseases using the provided ECG, CXR, and LAB information. Qwen2.5-VL-3B-Instruct can analyze different modalities but lacks accuracy and cannot summarize diseases. InternVL3-1B combines modality information to determine disease types, though its accuracy is lacking. LLaVA-One-Vision-7B refuses to answer questions.